ARTICLE

Theoretical Study of Isomerization and Decomposition Reactions for Methyl-nitramine

Wen-mei Wei[a], Ren-hui Zheng[a], Yan Tian[a], Tian-jing He[a*], Li He[b], Dong-ming Chen[a], Fan-chen Liu[a]

a. Department of Chemical Physics; b. Department of Electronic Science and Technology, University of Science and Technology of China, Hefei 230026, China

(Dated: Received on June 28, 2006; Accepted on September 5, 2006)

The complex potential energy surface and reaction mechanisms for the unimolecular isomerization and decomposition of methyl-nitramine (CH_3NHNO_2) were theoretically probed at the QCISD(T)/6-311+G*//B3LYP/6-311+G* level of theory. The results demonstrated that there are four low-lying energy channels: (i) the N–N bond fission pathway; (ii) a sequence of isomerization reactions via $CH_3NN(OH)O$; (IS2a); (iii) the HONO elimination pathway; (iv) the isomerization and the dissociation reactions via CH_3NHONO (IS3). The rate constants of each initial step (rate-determining step) for these channels were calculated using the canonical transition state theory. The Arrhenius expressions of the channels over the temperature range 298-2000 K are $k_6(T)=10^{14.8}e^{-46.0/RT}$, $k_7(T)=10^{13.7}e^{-42.1/RT}$, $k_8(T)=10^{13.6}e^{-51.8/RT}$ and $k_9(T)=10^{15.6}e^{-54.3/RT}$ s^{-1}, respectively. The calculated overall rate constants is 6.9×10^{-4} at 543 K, which is in good agreement with the experimental data. Based on the analysis of the rate constants, the dominant pathway is the isomerization reaction to form $CH_3NN(OH)O$ at low temperatures, while the N–N bond fission and the isomerization reaction to produce CH_3NHONO are expected to be competitive with the isomerization reaction to form $CH_3NN(OH)O$ at high temperatures.

Key words: Methyl-nitramine, Potential energy surface, Reaction mechanism, Canonical transition state theory, Rate constant

I. INTRODUCTION

The properties and reactions of nitro-containing compounds have been extensively studied [1-5] both theoretically and experimentally in recent years for the significant role they play in propellant ignition, combustion, and atmosphere pollution. The initial step in thermal decomposition of nitro-containing compounds is often the cleavage of the C–NO_2 or N–NO_2 bond [6]. In the unimolecular decomposition of dimethylnitramine (DMNA), however, three possible unimolecular pathways have been identified by McQuaid *et al*. [7]:

$$(CH_3)_2NNO_2 \rightarrow (CH_3)_2N + NO_2 \quad \text{(R1)}$$

$$(CH_3)_2NNO_2 \rightarrow (CH_3)_2NONO \quad \text{(R2)}$$

$$(CH_3)_2NNO_2 \rightarrow [TS] \rightarrow CH_2N(CH_3)_2 + NO_2H \quad \text{(R3)}$$

However, less is known about the unimolecular decomposition pathways of compounds with substitution of a methyl group for a hydrogen atom in the DMNA molecule, namely methyl-nitramine (CH_3NHNO_2). As a typical energetic molecule with modest size, the energetic and structural properties of methyl-nitramine can be studied in detail at high-level of theory. Dakhis *et al*. and Li *et al*. calculated and analyzed the normal vibrations of methyl-nitramine [8,9]. Using semi-empirical UHF-SCF-AM1 and PM3 methods, Fan *et al*. obtained the potential energy curves of the N–N bonds for NH_2NO_2, CH_3NHNO_2 and $(CH_3)_2NNO_2$, and found that there is a parallel relationship between the bond order of the N–N bond in these molecules and the activation energy of their N–N bond breaking [10]. Melius *et al*. calculated the heats of formation and free energies for CH_3NHNO_2 and identified the molecular radical species which might arise from the decomposition process using BAC-MP4 method [11]. Based on the calculated values, they compared the N–N homolysis for methyl-nitramine decomposition with a five-center transition state pathway to the elimination of nitrous acid and found that the latter pathway has an activation energy of 169.7 kJ/mol, significantly less than that of the former pathway, 202.7 kJ/mol, the N–N bond energy.

$$CH_3NHNO_2 \rightarrow CH_3NH + NO_2 \quad \text{(R4)}$$
$$\Delta E = 202.7 \quad \text{kJ/mol}$$

$$CH_3NHNO_2 \rightarrow [TS] \rightarrow CH_2NH + HONO \quad \text{(R5)}$$
$$\Delta E = 169.7 \quad \text{kJ/mol}$$

Though the activation energy of (R4) is 33.0 kJ/mol higher than that of (R5), they pointed out that (R4) should play an important role as the initial decomposition step at high temperatures, while (R5) is only possible to occur at low temperatures. But they did not explore the isomerization reaction processes for CH_3NHNO_2 and the possibility of rearrangement to an isomer just as the reaction (R2) of DMNA. Furthermore, the specific geometry parameters and the imaginary frequency of the so-called five-center tran-

*Author to whom correspondence should be addressed. E-mail: tj16@ustc.edu.cn

sition state were not reported, either. Kekin *et al.* studied the kinetics of the thermal decomposition of CH_3NHNO_2under isothermal conditions by a manometric method using a glass compensation manometer, and inferred that it proceeds by a radical mechanism with the primary cleavage of the N–N bond at a temperature of 503-543 K and a pressure of 30-56) kPa [12]. The N–N bond energy for CH_3NHNO_2 was reported by Wu *et al.* and Harris *et al.* at different levels of theory, respectively [13,14]. It is obvious that we are lacking in adequate scientific information about the reaction mechanisms and kinetics for methys-nitramine.

The present work investigated the detailed potential energy surface of methyl-nitramine at QCISD(T)/6-311+G*//B3LYP/6-311+G* level of theory, in an attempt to elucidate the mechanisms of the isomerization and decomposition of methyl-nitramine in gas phase. In conjunction with the canonical transition state theory, the rate constants of the initial steps (rate-determining steps) of the feasible reaction channels involved in the reactions are calculated. Based on the calculated results, the possible reaction mechanisms of methyl-nitramine were proposed.

II. METHODOLOGY

A. Computational details

Previous studies showed that the hybrid density functional theory (DFT) methods based on Becke's three-parameter functional can excellently reproduce the experimental results of the geometry and IR frequencies for nitramines [13,15,16]. In this work, with Becke's three-parameter hybrid exchange functional and the LYP correlation functional (B3LYP) in conjunction with the basis set 6-311+G*, geometry optimization of all reactants (IS), intermediates (IM), transition states (TS) and products was performed [17,18]. The characteristic of these structures and their zero-point vibrational energies (ZPE, scaled by a factor of 0.96 [19]) were determined from the frequency calculations at the same level. The optimized structure on the potential energy surface can be characterized as a transition state if only one imaginary frequency exists, or as a minimum if all non-zero frequencies are real. Intrinsic reaction coordinate (IRC [20]) calculations were traced to ensure that the transition states did in fact connect the proper minima. The potential energy surface for methyl-nitramine decomposition was calculated using the quandratic configuration interaction level of theory with single, double, and triple excitations (QCISD(T)) [21] with the same basis set as Johnson *et al.* [15] suggested that geometry optimizations using DFT methods followed by energy refinements to QCISD or QCISD(T) levels are recommended for the efficient and accurate calculation of nitramine reaction energies. In this work, we have also carried out additional calculations in some cases using CCSD(T)/6-311+G* method to confirm the energies obtained by the QCISD(T)/6-311+G* method and the results were in excellent agreement with each other. All calculations were performed with the Gaussian 98 package [22].

B. Rate constant calculations

Canonical transition state theory (CTST) [23,24] including a semiclassical one-dimensional multiplicative tunneling correction factor was used to predict the temperature dependence of the rate constants. The rate constants were computed using the following expression:

$$k(T) = \Gamma(T)\frac{k_b T}{h}\frac{Q_{TS}(T)}{Q_A(T)Q_B(T)}\exp\frac{-E_0}{k_b T} \qquad (1)$$

where $\Gamma(T)$ is the tunnelling correction factor at temperature T, $Q_{\rm TS}(T)$, $Q_{\rm A}(T)$ and $Q_{\rm B}(T)$ are the total partition functions for the transition state,the reactants A and B, respectively. E_0, k_b and h are the energy barrier, Boltzman's constant and Planck's constant, respectively. We adopted the simple and computationally inexpensive Wigner method [25] in the estimation of the tunneling corrections for the reactions:

$$\Gamma(T) = 1 + \frac{1}{24}\left(\frac{h\nu^{\neq}}{k_b T}\right)^2 \qquad (2)$$

where $\nu^{\neq}$ is the imaginary frequency at the saddle point. The rate constants were calculated at 101.3 kPa.

III. RESULTS AND DISCUSSION

Fifteen distinct decomposition pathways have been studied for methyl-nitramine. The optimized geometries of stationary points are depicted in Fig.1. The relative energies at QCISD(T) level of theory of the stationary points, which included the zero-point vibrational energy corrections calculated at the B3LYP/6-311+G* level, are presented in Table I. Unless specified, the relative energies with zero-point vibrational energy correction at QCISD(T) level of theory are used in the following discussions. The vibrational frequencies for the important stationary points are listed in Table II. The schematic profile of the potential energy surface at QCISD(T)//B3LYP for the most feasible isomerization and dissociation reactions of methyl-nitramine is plotted in Fig.2(a). Figure 2(b) displays the potential energy surface of the unfavorable isomerization and dissociation channels of methyl-nitramine, respectively.

A. Isomerizations of CH_3NHNO_2

CH_3NHNO_2 can take various isomerization followed by final decomposition. We first study the complex isomerization pathways from the isomer IS1 (Scheme 1).

IS1, CH_3NHNO_2. In the optimized geometry for CH_3NHNO_2, the atoms N2, N6, O8 and O9 are almost

ISSN 1003-7713/DOI:10.1360/cjcp2007.20(2).126.9

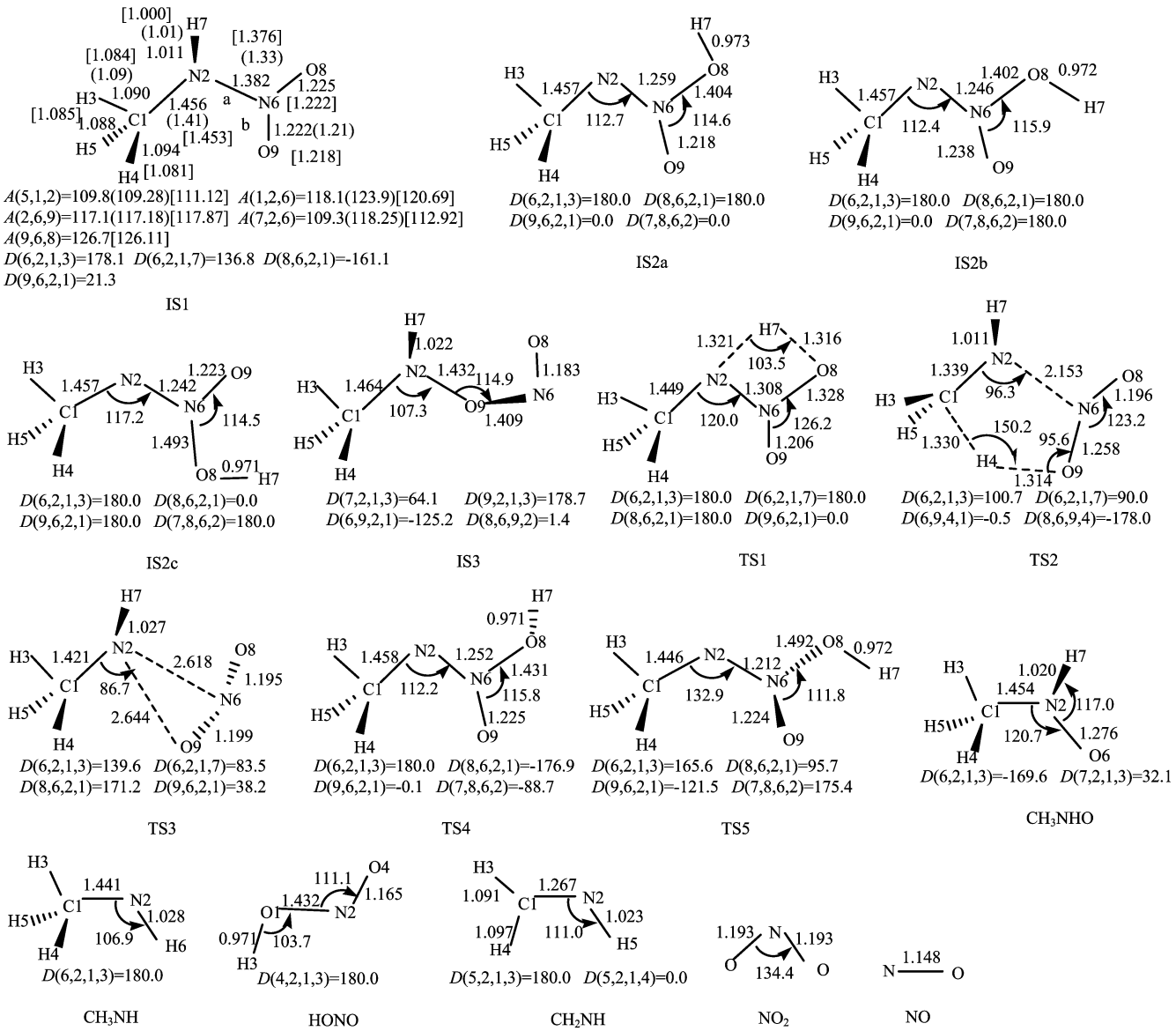

FIG. 1 Geometric parameters for some molecules at B3LYP/6-311+G* level of theory. Bond lengths are in angstroms, bond angles and dihedral angles are in degrees. The values in parenthesis are from Ref.[15]. The values in bracket are from Ref.[16].

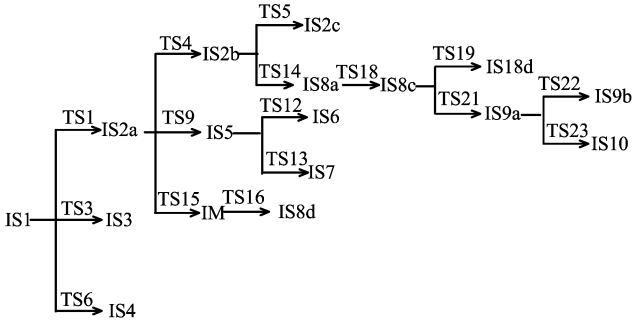

Scheme 1

at a plane, while the bonds C1–N2 and H7–N2 are protruded outside of the plane. From Fig.1 it can be seen that our calculations are in agreement with the experimental data [8], with the largest deviation of 0.05 Å in the N–N distance. Note that the data obtained in this work are in excellent agreement with that previously reported by Li *et al.* [9]. The measured vibrational frequencies in the experiment for CH_3NHNO_2 reported by Dakhis *et al.* [8] are 320, 595, 618, 727, 772, 928, 1092, 1097, 1177, 1332, 1394, 1434, 1454, 1470, 1614, 2923, 2953, 3016 and 3438 cm^{-1}, respectively, in which the two lowest ones have not been reported. The frequencies calculated at B3LYP/6-311+G* level listed in Table II agree well with the experimental results. We also located the triplet state equilibrium structure of

ISSN 1003-7713/DOI:10.1360/cjcp2007.20(2).126.9

TABLE I Zero-point vibrational energies (ZPE, at B3LYP/6-311+G* level, kJ/mol) and relative energies (in kJ/mol, RE1 at QCISD(T)/6-311+G* Level, RE2, at CCSD(T)/6-311+G* Level) for some species

Species	ZPE[a]	RE1[b]	RE2[c]	Species	ZPE[a]	RE1[b]	RE2[c]
IS1d	169.7	0.0	0.0	TS_{N-N}	148.4	187.3	
IS2a	167.2	40.5	40.1	TS1	154.2	175.6	176.0
IS2b	166.8	40.1	39.7	TS2	150.1	213.6	215.3
IS2c	165.9	52.2	52.7	TS3	149.6	216.9	
IS3	163.4	80.7	82.8	TS4	163.4	61.9	61.9
IS4	168.5	64.4		TS5	162.2	184.8	186.0
IS5	162.2	57.3		TS6	155.1	382.5	
IS6	164.3	34.3		TS7	147.6	245.4	
IS7	164.7	46.4		TS8	140.4	354.9	
IS8a	162.2	101.1		TS9	152.1	453.5	
IS8b	162.2	94.9		TS10	155.5	268.8	
IS8c	161.8	103.7		TS11	142.1	342.8	
IS8d	161.8	103.7		TS12	159.7	105.7	
IS9a	166.8	–69.4		TS13	154.7	263.3	
IS9b	165.5	–68.5		TS14	153.4	255.4	
IS10	166.8	69.0		TS15	144.2	335.2	
IM	157.6	–28.0		TS16	147.5	265.0	
$^2CH_3NH+^2NO_2$	145.0	186.8	188.5	TS17	142.1	263.7	
$^2CH_3+^2NHNO_2$	135.0	356.5		TS18	160.5	111.2	
$CH_2NH+HONO$	151.3	9.2	10.0	TS19	159.2	120.4	
CH_2O+NH_2NO	149.2	–46.4		TS20	145.5	268.8	
$^2CH_3NNO+^2OH$	144.6	218.2		TS21	155.1	276.3	
$CHNNOH+H_2O$	143.8	134.2		TS22	165.9	–49.7	
$CHOH+N_2+H_2O$	132.1	–98.6		TS23	152.1	196.5	
$^2CH_3NHO+^2NO$	151.3	104.9	104.5	TS24	144.6	266.3	
$^2CH_3+^2NN(OH)O$	135.4	368.7		TS25	148.0	79.8	
$^2CH_3+^2NHONO$	130.8	364.1					

[a] Calculated using B3LYP/6-311+G* method and scaled by a factor of 0.96.
[b] Values with zero-point vibrational energy correction at QCISD(T) /6-311+G*.
[c] Values with zero-point vibrational energy correction at CCSD(T)/6-311+G* level.
[d] The total energy is -299.70132 hartree.

^{3}IS1 at the same level of theory, in which the atoms C1, N2, H5 and H7 are almost at a plane, while the N6–N2 bond is protruded the plane. The dihedral angel of N6, N2, C1 and H7 atoms is 117.3°, while it is 136.8° in IS1. The bond lengths of C1–N2 , N2–N6, N6–O8 and N6–O9 bonds for ^{3}IS1 are 1.467, 1.428, 1.305 and 1.306 Å, respectively, longer by 0.011, 0.046, 0.080 and 0.084 Å than those in the structure of IS1, respectively. The energy of ^{3}IS1 lies 293.0 kJ/mol higher than the singlet IS1. Considering the much higher energy of the triplet state reactant, the possibility of its existence is very small. Therefore, the triplet pathways initiated by triplet state ^{3}IS1 contribute less compared with the singlet state IS1, and will not be discussed any more.

IS2, $CH_3NN(OH)O$. There are three Cs symmetry conformational isomers of $CH_3NN(OH)O$, i.e., IS2a, IS2b and IS2c. In their structures the atoms H3, C1, N2, N6, O8, O9 and H7 are at the same plane. The relative energies of them are 40.5, 40.1 and 52.2 kJ/mol, respectively. IS2a can isomerize to IS2b via a transition state TS4 with an imaginary frequency of 447i cm^{-1} and an energy barrier of 21.3 kJ/mol, which shows that it is easy for this reaction to occur. The barrier is in good agreement with the value of 21.7 kJ/mol calculated by CCSD(T)/6-311+G* method. This isomerization proceeds through a internal rotation of the H atom around the O8–H7 axis in IS2a and exothermic by 0.4 kJ/mol. Via TS5 with a barrier of 144.6 kJ/mol (146.3 kJ/mol at CCSD(T)/6-311+G* level) and an imaginary frequency of 354i cm^{-1}, IS2b can isomerize to IS2c by a rotating of the N(OH)O group around the N2–N6 axis. And it is predicted to be endothermic by 12.1 kJ/mol.

In the process of the isomerization from IS1 to IS2a

ISSN 1003-7713/DOI:10.1360/cjcp2007.20(2).126.9

TABLE II Vibrational frequencies and moments of inertia (10^{-40} g/cm^2) at the B3LYP/6-311+G* level for some species

	Frequencies[a]/cm^{-1}	I_A	I_B	I_C
IS1	134 178 292 515 563 719 751 910 1071 1105 1160 1299 1384 1413 1437 1468 1587 2917 2997 3031 3461	73.7	188.6	254.3
IS2a	159 237 298 424 521 623 696 898 996 1072 1144 1262 1305 1393 1434 1438 1620 2903 2955 3029 3542	73.6	189.1	257.5
IS2b	153 234 300 359 523 620 686 900 997 1068 1144 1234 1324 1394 1432 1439 1628 2903 2955 3031 3562	71.5	191.0	257.3
IS2c	155 228 319 411 535 596 667 712 1011 1068 1103, 1245 1286 1398 1441 1448 1663 2914 2971 3024 3569	77.6	183.1	255.4
IS3	36 214 295 349 462 632 735 850 953 992 1119 1208 1399 1433 1446 1471 1599 2897 2976 3010 3298	56.7	251.3	279.7
TS_{N-N}	131i 59 95 172 249 427 711 910 976 1053 1260 1283 1323 1372 1453 1623 2752 2882 2953 3290	85.5	461.9	536.1
TS1	1891i 77 147 276 602 683 697 894 944 1086 1129 1165 1312 1396 1431 1445 1536 2122 2907 2962 3028	80.0	182.2	256.9
TS2	1428i 177 257 341 491 505 589 796 932 1030 1039 1225 1228 1290 1324 1478 1485 1674 2906 3002 3330	73.6	244.5	309.5
TS3	486i 87 109 131 154 214 516 709 919 965 1033 1253 1281 1321 1398 1442 1618 2793 2816 2995 3261	81.4	279.0	343.6
TS4	447i 173 248 303 524 605 652 879 989 1062 1131 1236 1308 1383 1428 1437 1569 2901 2953 3031 3567	73.3	192.7	258.1
TS5	354i 125 185 444 470 508 671 727 911 1049 1102 1192 1335 1398 1443 1450 1724 2887 2943 3016 3556	81.6	210.8	273.0

[a] Scaled by a factor of 0.96.

via a four-membered ring transition state TS1, in which the breaking N2–H7 bond is elongated to 1.321 Å and the forming H7$\cdots$O8 bond is shortened to 1.316 Å. The process is endothermic by 40.5 kJ/mol. The transition state TS1 has an imaginary frequency of 1891i cm^{-1} and a barrier of 175.6 kJ/mol with respect to IS1. The energy barrier obtained at CCSD(T)/6-311+G* level of theory is 176.0 kJ/mol, clearly agreeing well with the QCISD(T)/6-311+G* results. This reaction process is confirmed by the IRC calculation.

IS3, CH_3NHONO. The relative energy of IS3 is 80.7 kJ/mol. IS1 can isomerize to IS3 through a three-membered ring transition state TS3 with an imaginary frequency of 485i cm^{-1} and a barrier of 216.9 kJ/mol. During this isomerization reaction, the distance between the N2 and O9 atoms in IS1a is gradually shortened and the N2–N6 bond is gradually elongated. In TS3, the breaking N2–N6 bond is elongated by 1.236 Å while the forming N2$\cdots$O9 bond is decreased to 2.644 Å. This isomerization reaction has been confirmed by IRC calculation and is predicted to be endothermic by 80.7 kJ/mol.

From Fig.2 (b) we can see that the barrier for IS1 isomerization to IS4 through a C1N2O6O9 four-membered ring transition state TS6 with an imaginary frequency of 611i cm^{-1} is 382.5 kJ/mol. IS2a transforms to IS5 via a N2O6O8 three-membered ring transition state TS9 with a 636i cm^{-1} imaginary frequency or transforms to IM via a C1H3N2 three-membered ring transition state TS15 with the 1, 2-H3 shift from C1-atom to N2-atom, the barriers in which are 413.0 and 294.7 kJ/mol, respectively. Clearly, the formations of the isomers IS4 and IS5 and the intermediate IM are energetically inaccessible and all these isomerizations are less favorable than those IS1 to IS2a and IS3. As can be seen from Fig.2 (b), though IS4, IS5 and IM can further convert to other isomers, these processes are kinetically unfavorable and then will not be discussed in detail.

B. Unimolecular decomposition pathways of CH_3NHNO_2

Fifteen dissociation pathways of CH_3NHNO_2 shown in Scheme 2 were investigated, Among them, Path 1, 3, 7 and 8 are the kinetically feasible dissociation paths, and we will discuss them in detail.

In Path 1 the direct N–N bond clevage of methylnitramine can lead to product CH_3NH and NO_2. Many researches showed that the N–N bond homolysis is the primary process in thermal decomposition of nitro-containing compounds [6,10,26,27]. No transition state is found for the simple N–N bond cleavage, and the N–N bond dissociation energy (BDE) calcu-

ISSN 1003-7713/DOI:10.1360/cjcp2007.20(2).126.9

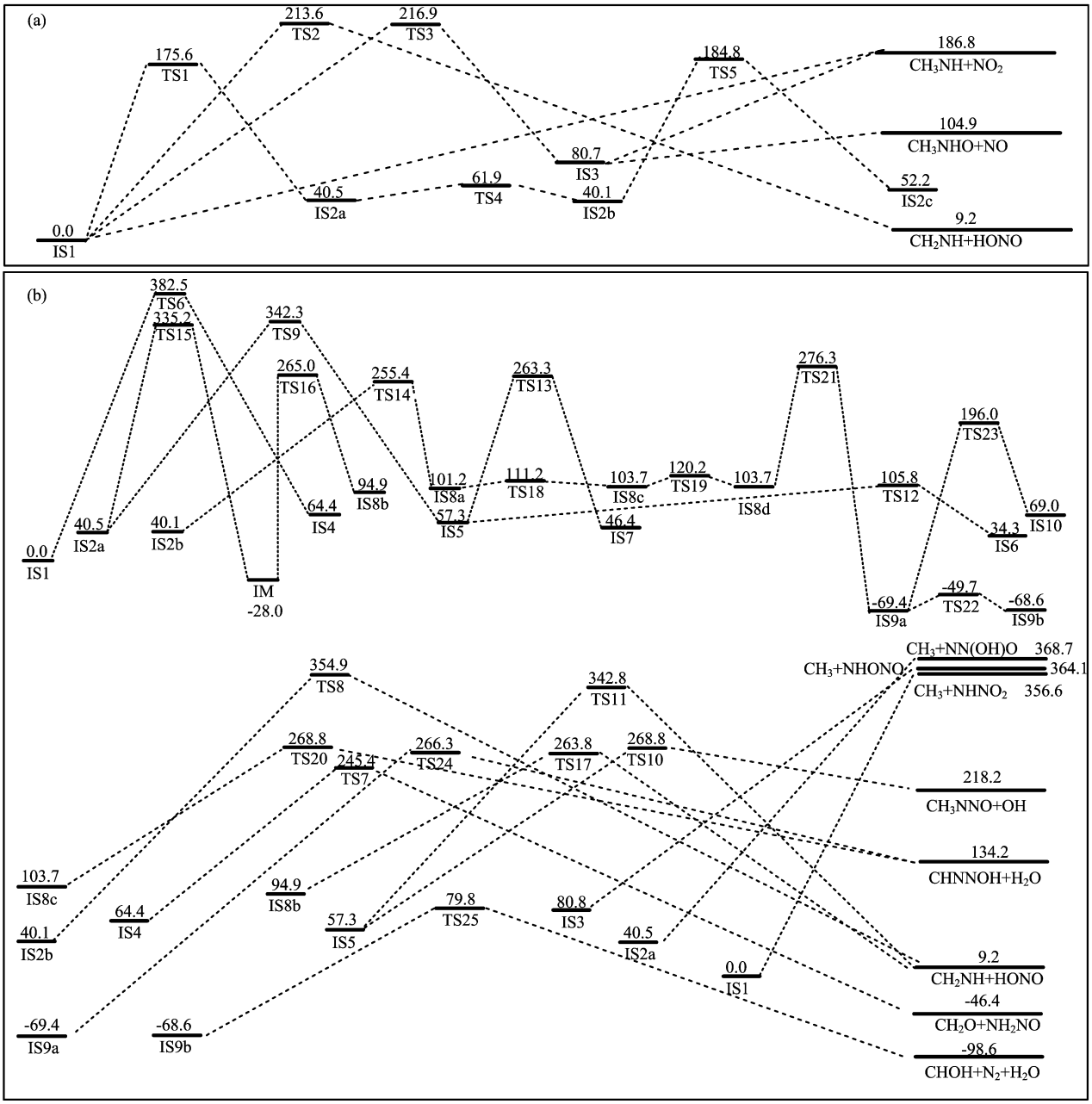

FIG. 2 (a) QCISD(T)//B3LYP potential energy diagram for the most feasible isomerization and dissociation reactions of methyl-nitramine. The energies are in kJ/mol; (b) QCISD(T)//B3LYP potential energy diagram for the unfavorable isomerization reactions of methyl-nitramine. The energies are in kJ/mol.

lated for CH_3NHNO_2 are 186.8 and 188.5 kJ/mol at the QCISD(T)//B3LYP and CCSD(T)//B3LYP level, respectively, which is in excellent agreement with the value of 186.0 kJ/mol reported by Harris *et al.* [14] at B3LYP/6-311G**level and a little smaller than the value of 216.1 kJ/mol at G2 level. In addition, our results agree very well with the values of 185.2 and 184.8 kJ/mol reported by Wu *et al.* [13] at B-PW91 and B3-LYP level, respectively, and with the value of 202.7 kJ/mol reported by Melius and Binkley [11] at BAC-MP4 level. No direct experimental value of the N–N BDE for CH_3NHNO_2 is available.

The concerted dissociation of methyl-nitramine to form CH_2NH and HONO in Path 3 is a complicated process involving the breaking and formation of multiple bonds. In going from reactant to products, the N2–N6 and C1–H4 bonds must break and O9–H4 bond must form. This process occurs through a five-membered ring transition state TS2 with an imaginary frequency of 1429i cm^{-1} and an energy barrier of 213.6 kJ/mol, which is 26.7 kJ/mol higher than N–N BDE. In TS2, the breaking C1–H4 and N2–N6 bonds are lengthened

ISSN 1003-7713/DOI:10.1360/cjcp2007.20(2).126.9

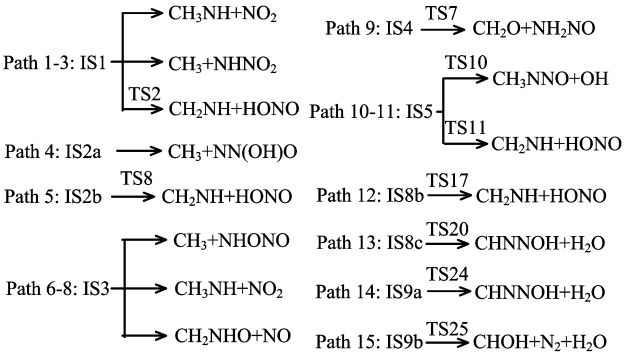

Scheme 2

to 1.330 and 2.153 Å, respectively, while the forming O9$\cdots$H4 bond is shortened to 1.314 Å. During this dissociation reaction, the H4 atom in CH_3NHNO_2 gradually moves to the O9 atom. IRC calculations have confirmed this path, which is predicted to be endothermic by 9.2 kJ/mol. To the best of our knowledge, only Melius *et al.* have reported this dissociation pathway based on the BAC-MP4 calculations [11], and the energy barrier calculated is 169.7, 43.9 kJ/mol smaller than ours and 33.0 kJ/mol lower than the N–N BDE calculated [11]. In order to clarify the notable discrepancy, we have carried out three additional calculations. The first one is the calculation of the barrier in Path 3 by using MP4/6-311+G* method, and a value of 211.5 kJ/mol is obtained, which is in excellent agreement with our results calculated at QCISD(T) (213.6 kJ/mol) and CCSD(T) (215.3 kJ/mol) levels. The second one is attempting to find the transition state connecting IS2a with CH_2NH+HONO because the barrier of 169.7 kJ/mol in Path 3 obtained by Melius is close to the barrier of TS1, that is 175.6 kJ/mol in the process from IS1 to IS2a in this study, but it failed. The last one is considering another possibility, in which the IS2a molecule first isomerizes to the isomer $CH_2NHN(OH)O$, then the isomer dissociates to the final products of CH_2NH and HONO. However, $CH_2NHN(OH)O$ is not stable at either B3LYP or MP2 level. Because there were no specific geometry parameters reported in Melius's results for the transition state and we can not further study to get a clear and unambiguous explanation and evaluation.

Starting from IS3 two dissociation reactions have been studied, namely Path 7 and 8, and both of them have no transition states. Path 7 is a direct N2–O9 bond homolysis in IS3 to form CH_3NH plus NO_2 and Path 8 is the O9–N6 bond clevage to give CH_3NHO and NO. The N2–O9 and O9–N6 BDEs in IS3 are 186.8 and 104.9 kJ/mol, respectively. The former process is predicted to be endothermic by 106.2 kJ/mol and the latter is endothermic by 24.2 kJ/mol.

From Fig.2 (b) we can see that the direct C-N rupture of CH_3NHNO_2 leading to CH_3 and $NHNO_2$ in Path 2 is barrierless and the C–N BDE is 356.5, 169.7 kJ/mol higher than the N–N BDE, which indicates this path is kinetically unfeasible. In Path 4, IS2a decomposes into CH_3 and NN(OH)O directly, the dissociation energy is 368.7 kJ/mol, much higher than those of the feasible decomposition path. In Path 5 the energy barrier of IS2b dissociation to CH_2NH and HONO via a three-membered ring transition state TS8 with an imaginary frequency of 398i cm^{-1} is as high as 314.7 kJ/mol. The C–N BDE in IS3 to produce CH_3 plus NHONO is 283.4 and 177.2 kJ/mol higher than that of the N2–O9 BDE in IS3. For the remaining paths, the reactant isomers are kinetically unfeasible to reach as being discussed above, the dissociation channels initiating from them will not been considered further more.

The results show that the most feasible isomerization and decomposition pathways for methyl-nitramine are:

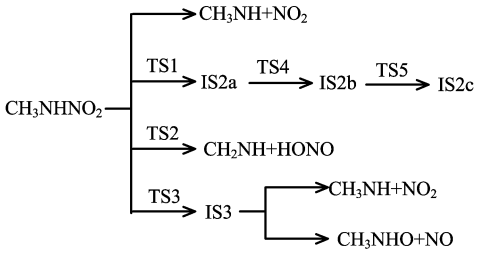

Their energies can be seen clearly in Fig.2 (a).

C. Rate constants

From the discussions above on the reaction mechanism of the unimolecular isomerization and dissociation of methyl-nitramine we can see that the rate-determing steps of the most feasible isomerization and decomposition pathways for methyl-nitramine are the initial steps:

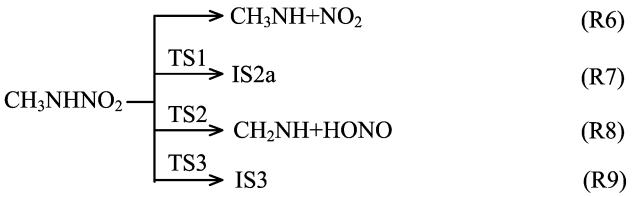

Kekin *et al.* also claimed that the measured rate constants for the thermal decomposition of CH_3NHNO_2 may be assigned to those of the initial, rate-limiting step in the decomposition [12]. Thus we calculated the rate constants using Eq.(1) and Eq.(2) for these elementary reactions and examined kinetic characteristics of the unimolecular decomposition of methyl-nitramine.

Since the N–N fission pathway, reaction (R6), is a barrierless reaction and has no classical well-defined transition state, we have to obtaine its generalized transition state on the QCISD(T)//B3LYP/6-311+G* potential energy surface using the microcanonical variational transition state theory [23]

$$\frac{\partial W(E, R_C)}{\partial R_C} = 0 \qquad (3)$$

ISSN 1003-7713/DOI:10.1360/cjcp2007.20(2).126.9

TABLE III Rate constants (s^{-1}) at the selected temperatures for the reactions (R6), (R7), (R8) and (R9).

Temperature/K	298	503	513	523	533	543	600	1000	1500
k_6	$1.2e^{-19}$	$6.8e^{-6}$	$1.7e^{-5}$	$4.0e^{-5}$	$9.2e^{-5}$	$2.0e^{-4}$	$1.2e^{-2}$	$6.5e^{4}$	$1.4e^{8}$
k_7	$7.9e^{-18}$	$2.3e^{-5}$	$5.1e^{-5}$	$1.1e^{-4}$	$2.4e^{-4}$	$4.9e^{-4}$	$1.9e^{-2}$	$2.6e^{4}$	$3.3e^{7}$
k_8	$5.5e^{-25}$	$9.2e^{-10}$	$2.5e^{-9}$	$6.6e^{-9}$	$1.7e^{-8}$	$4.0e^{-8}$	$3.7e^{-6}$	$1.3e^{2}$	$9.4e^{5}$
k_9	$8.4e^{-25}$	$8.0e^{-9}$	$2.3e^{-8}$	$6.3e^{-8}$	$1.7e^{-7}$	$4.3e^{-7}$	$5.0e^{-5}$	$4.3e^{3}$	$4.5e^{7}$
$k_{overall}$ [a]	$7.9e^{-18}$	$2.9e^{-5}$	$6.8e^{-5}$	$1.5e^{-4}$	$3.3e^{-4}$	$6.9e^{-4}$	$3.1e^{-2}$	$9.5e^{4}$	$2.2e^{8}$
k_{exp} [b]		$7.70e^{-5}$	$1.41e^{-4}$	$3.35e^{-4}$	$7.51e^{-4}$	$1.45e^{-3}$			

[a] $k_{overall}= k_6+k_7+k_8+k_9$; [b] Experimental data from Ref.[19].

where W is the number of states and R_C is the reaction coordinate. The calculations were carried out by fixing the reaction coordinates, R(N–N), but allowing the full optimization of the remained structural parameters [28]. Then the transition state, marked as TS_{N-N}, was located at the point of R(N–N)=3.05 Å.

Figure 3 shows the plots of the rate constants versus temperature (in the range of 298-2000 K) for these rate-determining reactions and the available theoretical and experimental data in the literature. It can be seen that our results are in good agreement with the experimental values. It is clear that the rate constants of all these reactions are strongly temperature-dependent, and the isomerization reaction to form $CH_3NN(OH)O$ (R7) dominates at low temperatures. However, with the increase of temperature, the rate constants of the N–N bond fission (R6) and the isomerization reaction to form CH_3NHONO (R9) increase more rapidly than the others reactions, and about at 500 K, (R6) becomes competitive with (R7). And the rate constant of (R6) is about the same as that of (R7) at a temperature of 600 K. When the temperature increases to about 1100 K, (R9) is competitive with (R6) and (R7). Finally, at 1400 K, the rate constant of (R9) is about the same as that of (R7). The results indicate that (R7) is the main favorable reaction at the temperature range of 298-500 K, and (R6) is competitive with (R7) at 500-1100 K, and (R6), (R7) and (R9) are competitive at the temperature higher than 1100 K. Although the HONO elimination pathway (R8) may compete with (R9) at low temperatures, the rate constants of (R8) are the slowest among these reactions in the whole temperature range. This result is different from that reported by Melius *et al.* [11], who indicated that it is possible to compete for the HONO elimination reaction with the direct N–N bond fission reaction at low temperatures based on the results at BAC-MP4 level of theory. The Arrhenius expressions obtained are $k_6(T)=10^{14.8}e^{-46.0/RT}$, $k_7(T)=10^{13.7}e^{-42.1/RT}$, $k_8(T)=10^{13.6}e^{-51.8/RT}$ and $k_9(T)=10^{15.6}e^{-54.3/RT}$ s^{-1} at the temperature range from 298 to 2000 K for reactions (R6), (R7), (R8) and (R9), respectively.

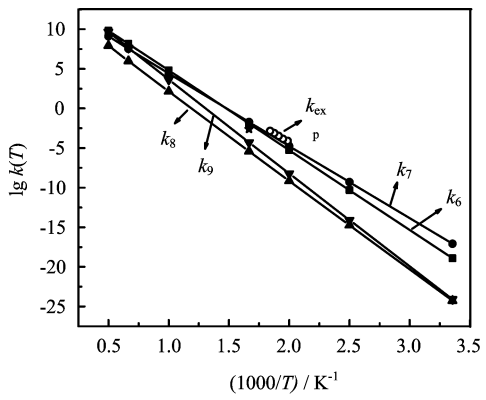

FIG. 3 Arrehenius plots of the rate constants of (R6), (R7), (R8) and (R9). Star and circles correspond to the theoretical and experimental data from Ref.[18] and [19], respectively.

Under isothermal conditions by a manometric method using a glass compensation manometer, Kekin *et al.* studied the kinetics of the thermal decomposition of CH_3NHNO_2 [12]. By measuring the concentration of the reactant, they obtained the overall rate constants in the temperature range of 503-543 K and at a pressure of 30-56 kPa. Table III lists the rate constants at the selected temperatures (In addition to the room temperature and experimental temperature values, we also list the rate constants at 600, 1000 and 1500 K because of the importance of these temperatures for decomposition and combustion conditions) and the experimental values for theses reactions. Obviously, the overall rate constants calculated by us are in good agreement with the experimental values. For example, the calculated rate constants at 503, 533 and 543 K are 2.9×10^{-5}, 3.3×10^{-4} and 6.9×10^{-4} respectively, while the corresponding experimental values are 7.70×10^{-5}, 7.51×10^{-4} and 1.45×10^{-3}, respectively. Kekin *et al.* suggested that the thermal decomposition of CH_3NHNO_2 should proceed via primary cleavage of the N–N bond in the temperature range of 503-543 K [12], while our results show that the isomerization reaction of CH_3NHNO_2 to $CH_3NN(OH)O$ may be competitive with the N–N bond homolysis in this temperature range. The suggestion of Kekin *et al.* were based on that the changing at the initial pressure P_0 and the

ISSN 1003-7713/DOI:10.1360/cjcp2007.20(2).126.9

S/V (cm^{-1}) did not lead to the change in the decomposition rate of CH_3NHNO_2 and the analogy to the well established mechanism for secondary nitroamines [12]. However, neither of them can exclude the possibility of the isomerization reaction.

Note that the rate constants of HONO elimination path (R8) at a temperature of 600 K is 3.7×10^{-6} s^{-1} in this work, which is about 10^3 smaller than that (2.5×10^{-3} s^{-1}) reported by Melius *et al.* [11]. This difference may result from the energy barrier discrepancy calculated. The barrier based on the BAC-MP4 method by Melius *et al.* is 43.9 kJ/mol, smaller than ours as discussed above. There are not yet the direct experimental data of rate constant for (R8) in the literature. However, Kekin *et al.* reported that the experimental rate constant of CH_3NHNO_2 dissociation was 1.45×10^{-3} s^{-1} at 543 K [12]. The rate constants of (R6), (R7), (R8) and (R9) calculated by us at 543 K are 2.0×10^{-4}, 4.9×10^{-4}, 4.0×10^{-8} and 4.3×10^{-7} s^{-1}, respectively, and the overall rate constant calculated is 6.9×10^{-4} at 543 K. These results indicate the calculated rate constants are in good agreement with the corresponding experimental values.

IV. CONCLUSION

The potential energy surface and reaction mechanisms of the isomerization and decomposition of methyl-nitramine were calculated at the QCISD(T) /6-311+G*//B3LYP/6-311+G* level of theory. The calculated results demonstrate that there are four low-lying energy channels, and among them one channel belongs to the N–N bond fission pathway, one belongs to the HONO elimination pathway and the others belong to the isomerization reactions. The rate constants of these feasible reactions were calculated using CTST theory. The Arrhenius expressions of these channels in the temperature range from 298K to 2000 K are $k_6(T)=10^{14.8}e^{-46.0/RT}$, $k_7(T)=10^{13.7}e^{-42.1/RT}$, $k_8(T)=10^{13.6}e^{-51.8/RT}$ and $k_9(T)=10^{15.6}e^{-54.3/RT}$ s^{-1}, respectively. The calculated overall rate constants is 6.9×10^{-4} at 543 K, which is in good agreement with the experimental data. Based on the analyses of the rate constants, the dominant pathway is the isomerization reaction to form $CH_3NN(OH)O$ at low temperatures, while the N–N bond fission and the isomerization reaction to produce CH_3NHONO are expected to be competitive with the isomerization reaction to form $CH_3NN(OH)O$ at high temperatures.

V. ACKNOWLEDGMENT

This work was supported by the National Natural Science Foundation of China (No.20473078).

[1] W. F. Hu, T. J. He, D. M. Chen and F. C. Liu, J. Phys. Chem. A **106**, 7294 (2002).
[2] W. M. Wei, W. Tan, R. H. Zheng, T. J. He, D. M. Chen and F. C. Liu, Chem. Phys. **312**, 241 (2005).
[3] W. M. Wei, W. Tan, T. J. He, D. M. Chen and F. C. Liu, Chin. J. Chem. Phys. **17**, 679 (2004).
[4] W. M. Wei, R. H. Zheng, Y. Tian, T. J. He, D. M. Chen and F. C. Liu, Acta Phys. Chim. Sin. **53**, 22 (2006).
[5] X. Zhang, R. Kan, Y. Liu, K. P and H. Li, Chin. J. Chem. Phys. **17**, 561 (2004).
[6] R. Guirguis, D. Hsu, D. Bogan and E. Oran, Combust. Flame **61**, 51 (1985).
[7] M. J. McQuaid, A. W. Miziolek, R. C. Sausa and C. N. Merrow, J. Phys. Chem. **95**, 2713 (1991).
[8] M. I. Dakhis, V. G. Dashevsky and V. G. Avakyan, J. Mol. Struct. **13**, 339 (1972).
[9] Y. Li, H. Xiao, W. Wang and K. Fan, Acta. Chim. Sin. **50**, 1063 (1992).
[10] J. Fan, H. Xiao, Y. Li and S. Hong, Energetic Materials (Chinese) **3**, 1 (1995).
[11] C. F. Melius and J. S. Binkley, Twenty-first Symposium (International) on Combustion, Proceedings, The Combustion Institute, 1953 (1986).
[12] Y. U. Kekin, V. N. Shan'ko and R. S. Stepanov, Kinet. Catal. **30**, 848 (1989).
[13] C. J. Wu and L. E. Fried, J. Phys. Chem. A **101**, 8675 (1997).
[14] N. J. Harris and K. Lammertsma, J. Am. Chem. Soc. **119**, 6583 (1997).
[15] M. A. Johnson and T. N. Truong, J. Phys. Chem. A **103**, 8840 (1999).
[16] A. Gindulytė, L. Massa, L. Huang and J. Karle, J. Phys. Chem. A **103**, 11040 (1999).
[17] A. D. Becke, J. Chem. Phys. **98**, 5648 (1993).
[18] C. Lee, W. Yang and R. G. Parr, Phys. Rev. B **37**, 785 (1988).
[19] J. B. Foresman and A. Frisch, *Exploring Chemistry with Electronic Structure Methods*, 2nd Edn., Pittsburgh, PA: Gaussian, Inc., 64 (1995).
[20] C. Gonzalez and H. B. Schlegel, J. Chem. Phys. **90**, 2154 (1989).
[21] J. A. Pople, M. Head-Gordon and K. Raghavachari, J. Chem. Phys. **87**, 5968 (1987).
[22] M. J. Frisch et al., GAUSSIAN 98, Revision A.11, Pittsburgh, PA: Gaussian, Inc., (2001).
[23] J. I. Steinfeld, J. S. Francisco and W. L. Hase, *Chemical Kinetics and Dynamics*, Englewood Cliffs, NJ: Prentice Hall, (1989).
[24] D. G. Truhlar, B. C. Garrett and S. J. Klippenstein, J. Phys. Chem. **100**, 12771 (1996).
[25] E. P. Wigner, Z. Phys. Chem. **B19**, 203 (1932).
[26] R. Shaw and F. E. Walker, J. Phys. Chem. **81**, 2572 (1977).
[27] S. Zhang, H. N. Nguyen and T. N. Truong, J. Phys. Chem. A **107**, 2981 (2003).
[28] E. Drougas, D. K. Papayannis and A. M. Kosmas, Chem. Phys. **276**, 15 (2002).

ISSN 1003-7713/DOI:10.1360/cjcp2007.20(2).126.9